A new class of fatty acid allene oxide formed by the DOX-P450 fusion proteins of human and plant pathogenic fungi, *C. immitis* and *Z. tritici*

Ernst H. Oliw,[1] Marc Aragó, Yang Chen, and Fredrik Jernerén

Division of Biochemical Pharmacology, Department of Pharmaceutical Biosciences, Uppsala University, SE-751 24 Uppsala, Sweden

Abstract **Linoleate dioxygenase-cytochrome P450 (DOX-CYP) fusion enzymes are common in pathogenic fungi. The DOX domains form hydroperoxy metabolites of 18:2*n*-6, which can be transformed by the CYP domains to 1,2- or 1,4-diols, epoxy alcohols, or to allene oxides. We have characterized two novel allene oxide synthases (AOSs), namely, recombinant 8*R*-DOX-AOS of *Coccidioides immitis* (causing valley fever) and 8*S*-DOX-AOS of *Zymoseptoria tritici* (causing septoria tritici blotch of wheat). The 8*R*-DOX-AOS oxidized 18:2*n*-6 sequentially to 8*R*-hydroperoxy-9*Z*,12*Z*-octadecadienoic acid (8*R*-HPODE) and to an allene oxide, 8*R*(9)-epoxy-9,12*Z*-octadecadienoic acid, as judged from the accumulation of the α-ketol, 8*S*-hydroxy-9-oxo-12*Z*-octadecenoic acid. The 8*S*-DOX-AOS of *Z. tritici* transformed 18:2*n*-6 sequentially to 8*S*-HPODE and to an α-ketol, 8*R*-hydroxy-9-oxo-12*Z*-octadecenoic acid, likely formed by hydrolysis of 8*S*(9)-epoxy-9,12*Z*-octadecadienoic acid. The 8*S*-DOX-AOS oxidized [8*R*-^{2}H]18:2*n*-6 to 8*S*-HPODE with retention of the ^{2}H-label, suggesting suprafacial hydrogen abstraction and oxygenation in contrast to 8*R*-DOX-AOS. Both enzymes oxidized 18:1*n*-9 and 18:3*n*-3 to α-ketols, but the catalysis of the 8*R*- and 8*S*-AOS domains differed. 8*R*-DOX-AOS transformed 9*R*-HPODE to epoxy alcohols, but 8*S*-DOX-AOS converted 9*S*-HPODE to an α-ketol (9-hydroxy-10-oxo-12*Z*-octadecenoic acid) and epoxy alcohols in a ratio of ~1:2. Whereas all fatty acid allene oxides described so far have a conjugated diene impinging on the epoxide, the allene oxides formed by 8-DOX-AOS are unconjugated.—** Oliw, E. H., M. Aragó, Y. Chen, and F. Jernerén. **A new class of fatty acid allene oxide formed by the DOX-P450 fusion proteins of human and plant pathogenic fungi, *C. immitis* and *Z. tritici*. *J. Lipid Res.* 2016.** 57: **1518–1528.**

Supplementary key words cyclooxygenase • cytochrome P450 74 family • 8-dioxygenase • lipidomics • lipid metabolism • oxygenation mechanism • dioxygenase • *Coccidioides immitis* • *Zymoseptoria tritici*

Eicosanoids in humans and oxylipins in plants and fungi designate oxygenated unsaturated C_{20} and C_{18} fatty acids and many of them exert potent biological actions (1–3). Fungal oxylipins can be formed by dioxygenation of C_{18} fatty acids by two groups of enzymes, lipoxygenases (LOXs) and heme-containing dioxygenases (DOXs) (2). The LOXs contain catalytic Fe or Mn, and oxidize unsaturated fatty acids to hydroperoxides by hydrogen abstraction at *bis*-allylic positions (4–8). The heme-containing DOXs belong to the cyclooxygenase (COX) gene family (9). They can oxidize fatty acids at allylic as well as *bis*-allylic positions due to hydrogen abstraction by a tyrosyl radical (10, 11).

The first characterized fungal DOX related to COX was 7,8-linoleate diol synthase (LDS) (12, 13). The 7,8-LDS is a fusion protein with an 8*R*-DOX domain and a C-terminal cytochrome P450 (CYP) domain with the 7,8-LDS activities (14). This enzyme and the related 5,8- and 8,11-LDSs can be collectively labeled 8*R*-DOX-LDS for simplicity. There are now five additional characterized groups of enzymes with sequence homology to 8*R*-DOX-LDS. They usually align with over 60% amino acid sequence identities within each group. The transformation of 18:2*n*-6 by all eight enzymes is outlined in **Fig. 1A**. The DOX domains form 8*R*-, 9*R*-, 9*S*-, and 10*R*-hydroperoxy metabolites of 18:2*n*-6 and 18:3*n*-3 (14–17). The C-terminal CYP domains can transform these hydroperoxides by heterolytic cleavage leading to intramolecular hydroxylation at C-7, C-5, or C-11 with formation of 1,2- or 1,4-diols by 8*R*-DOX-LDS or epoxidation of the *n*-6 double bond by 10*R*-DOX-epoxy alcohol synthases (10*R*-DOX-EASs). The 9*R*- and 9*S*-hydroperoxides

Abbreviations: AOS, allene oxide synthase; CP, chiral-phase; COX, cyclooxygenase; CYP, cytochrome P450; DiHODE, dihydroxyoctadecadienoic acid; DOX, dioxygenase; EAS, epoxy alcohol synthase; EODE, epoxyoctadecadienoic acid; HPODE, hydroperoxyoctadecadienoic acid; HPOTrE, hydroperoxyoctadecatrienoic acid; LDS, linoleate diol synthase; LOX, lipoxygenase; NP, normal-phase; SRS, substrate recognition site; RP, reversed-phase; TPP, triphenylphosphine; α-ketol, C_{18} fatty acids with 8-hydroxy-9-oxo- or 9-hydroxy-10-oxo structural elements.

[1] To whom correspondence should be addressed.
e-mail: Ernst.oliw@farmbio.uu.se

[S] The online version of this article (available at http://www.jlr.org) contains a supplement.

This work was supported by Vetenskapsrådet Grant K2013-67X-06523-31-3 and the Knut and Alice Wallenberg Foundation Grant KAW 2004.0123. M.A. was supported by the Erasmus program.

Manuscript received 4 May 2016 and in revised form 9 June 2016.

Published, JLR Papers in Press, June 9, 2016
DOI 10.1194/jlr.M068981

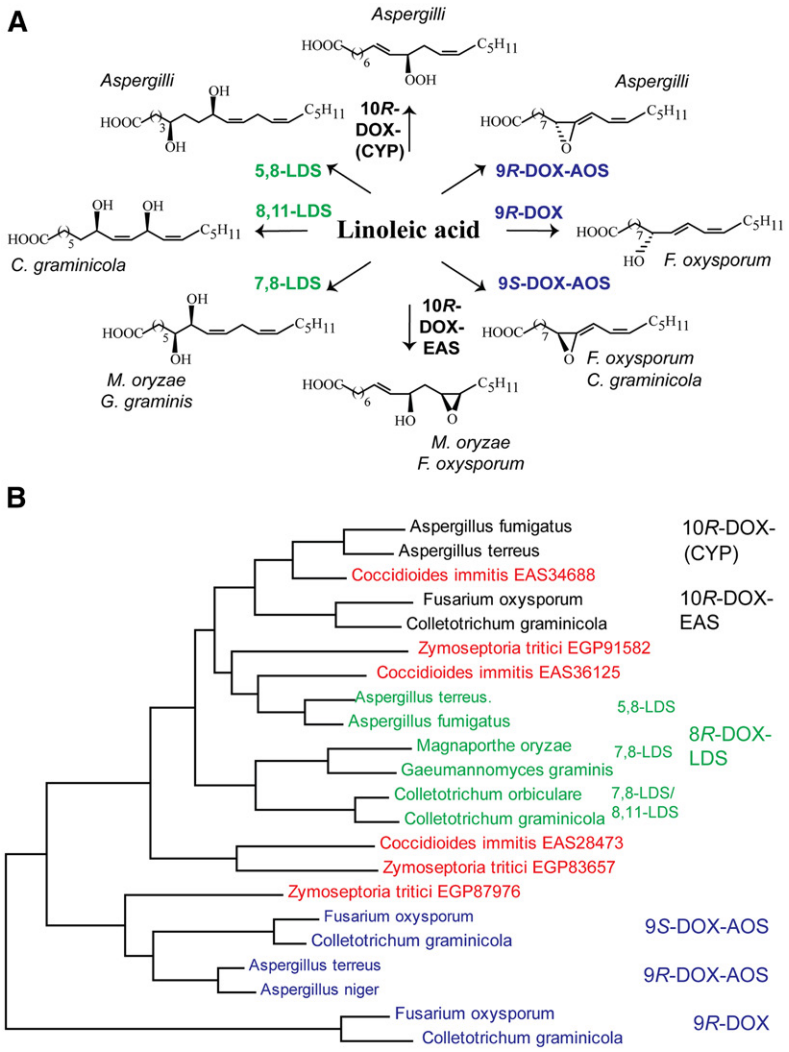

Fig. 1. Overview of oxylipins formed by DOX-CYP and related enzymes and their sequence similarities. A: Overview of fungal oxylipins formed by DOX-CYP fusion enzymes. Linoleic acid is transformed by mycelia and/or by recombinant enzymes of subfamilies of DOX-CYP fusion to 1,2- and 1,4-diols (left, marked green), to allene oxides (right, marked blue), to an epoxy alcohol (bottom, black), and to 10*R*-HPODE (top, black). The parentheses in 10*R*-DOX-(CYP) indicate that the CYP domain is homologous to P450 but lacks the critical Cys residue for catalysis. B: Phylogenetic tree of characterized DOX-CYP fusion enzymes except for three orphans each of *C. immitis* and *Z. tritici* (marked red). The sequences are (GenBank identification numbers): EDP52540 and AFB71131 for 10*R*-DOX-(CYP); EGU86021 and EFQ36272 for 10*R*-DOX-EAS; for three subfamilies of 8*R*-DOX-LDS: AGA95448 and EDP50447 for 5,8-LDS, EHA52010 and Q9UUS2 for 7,8-LDS, KDN68726 and EFQ34869 for 7,8- and 8,11-LDS; EGU88194 and EFQ27323 for 9*S*-DOX-AOS; AGH14485 and EHA29500 for 9*R*-DOX-AOS; EGU79548 and EFQ36675 for 9*R*-DOX.

of 18:2*n*-6 can also be subject to homolytic cleavage and dehydration to allene oxides by allene oxide synthases (AOSs) (9*R*- and 9*S*-DOX-AOS) (Fig. 1A). AOSs of plants belong to the CYP74 family, but the fungal AOSs form separate CYP families (17, 18). The 8*R*-DOX-LDS is often expressed by mycelia in laboratory cultures of many strains, whereas other DOX-CYP may be expressed by certain strains or only in response to specific environmental stimuli (1, 19).

The DOX-CYP enzymes can also be classified from the position of hydrogen abstraction of linoleic acid: C-8 by 8*R*- and 10*R*-DOX and C-11 by 9-DOX (12, 15, 17). The general theme is antarafacial hydrogen abstraction and oxygen insertion in analogy with COX, but there are two exceptions: 9*R*-DOX and 9*R*-DOX-AOS (17, 18, 20).

Coccidioides immitis causes valley fever in Western USA with occasionally lethal outcomes (21). *Zymoseptoria tritici* (teleomorph *Mycosphaerella graminicola*) causes the most important disease of wheat, septoria tritici blotch (22, 23). Little is known about the DOX-CYP enzymes of these important pathogens. Fungal oxylipins may take part as secondary metabolites in sporulation, the infectious processes, and in biotrophic and necrotic growth (1, 2). It therefore seemed of interest to determine whether *C. immitis* and *Z. tritici* might code for known or unique enzymes with homology to 8*R*-DOX-LDS and related enzymes.

C. immitis and *Z. tritici* code for three DOX-CYP fusion enzymes each. These tentative proteins can be aligned with characterized DOX-CYP, as shown by the phylogenetic tree in Fig. 1B. The alignment suggests that EGP91582 and EAS36125 are likely related to 8*R*-DOX-LDS. EAS34688 is connected to 10*R*-DOX-(CYP), but EAS34688 retains the heme-thiolate cysteine in the CYP domain in contrast to 10*R*-DOX-(CYP) and might therefore be catalytically related to the nearby 10*R*-DOX-EAS subfamily (see Fig. 1B). The catalytic properties of the three remaining enzymes are more difficult to deduce.

EAS28473 and EGP83657 appear to be only distantly related to the known DOX-CYP subfamilies, but they can be aligned with 51% amino acid identity (Fig. 1B). EGP87976 aligns with both 9*R*- and 9*S*-DOX-AOS, and could be catalytically related. All three proteins have conserved the proximal and distal His heme ligands and the catalytically important Tyr residue in the DOX domains and the critical heme thiolate cysteine in the CYP domains.

We decided to express and characterize EAS28473, EGP83657, and EGP87976 for three reasons. First, they appeared to form, on sequence alignment with related

enzymes, at least one separate subfamily (Fig. 1B). Second, the sequence information deduced from the DOX and CYP domains did not allow any unambiguous conclusions on their dual catalytic activities. Third, *C. immitis* and *Z. tritici* are important pathogens, and characterization of novel enzymes might provide important information for future biological studies (1, 2). Work with mycelia of *C. immitis* has caused fatal infections in laboratory personnel (21), but we assessed the oxidation of fatty acids by mycelia of *Z. tritici*.

EXPERIMENTAL PROCEDURES

Materials

Fatty acids were dissolved in ethanol and stored in stock solutions (35–100 mM) at −20°C. The 18:2*n*-6 (99%), 18:3*n*-6 (99%), and 18:3*n*-3 (99%) were from VWR, and 18:1*n*-9, 20:2*n*-6, 20:4*n*-6, and [$^{13}C_{18}$]18:2*n*-6 (98%) were from Larodan (Malmö, Sweden). The [11*S*-^{2}H]18:2*n*-6 (>99% ^{2}H) and [8*R*-^{2}H]18:2*n*-6 (65% ^{2}H) were prepared by Dr. Hamberg as described (24). The 9*S*-hydroperoxyoctadecatrienoic acid (HPOTrE) and 9*R*-, 9*S*-, 13*R*-, and 13*S*-hydroperoxyoctadecadienoic acids (HPODEs) were prepared by potato and tomato LOX and by 13*R*-MnLOX (17). The 8*S*-, 8*R*-, and 12*S*-HETE were from Cayman. The $^{18}O_2$ (97%), RNaseA, lysozyme, DNase I, and ampicillin were from Sigma. The [$^{13}C_{18}$]8*R*-HPODE was prepared with the 8*R*-DOX domain of 7,8-LDS (14). The [$^{18}O_2$]8*R*-HPODE (>95% ^{18}O) was prepared in the same way by incubation under $^{18}O_2$. The labeled 8*R*-HPODE was purified by reversed-phase (RP)-HPLC. Chemically competent *Escherichia coli* (NEB5α) were from New England BioLabs. Champion pET101D Directional TOPO kit was from Invitrogen. Restriction enzymes and the gel extraction kit were from Fermentas. Sequencing was performed at Uppsala Genome Center (Uppsala University). The open reading frames of GenBank EAS28473 (*C. immitis*), EGP83657 (*Z. tritici*), and EGP87976 (*Z. tritici*) in pUC57 vectors were purchased from GenScript (Piscataway, NJ). PCR primers were ordered from TIB Molbiol (Berlin, Germany). SepPak columns (silicic acid and C_{18} silica) were from Waters. *Z. tritici* IPO323 (CBS 115943) was obtained from CBS-KNAW Fungal Biodiversity Centre (Utrecht, The Netherlands). *Z. tritici* was first grown on agar plates (V8 or potato dextrose) and then transferred to 100 ml medium (1 g yeast extract and 3 g glucose per liter) with shaking at room temperature or 18°C for 10–12 days (23). Mycelia were harvested by filtration, ground to a fine powder in a mortar with liquid N_2, and stored at −80°C.

Expression of recombinant proteins

The open reading frames of EAS28473, EGP83657, and EGP87976 in pUC57 were transferred to pET101D-TOPO vectors by PCR technology according to Invitrogen's instructions. Competent *E. coli* (BL21 Star) cells were transformed with the expression constructs by heat shock (16). Cells were grown for 2–3 h at 37°C until they obtained an A_{600} of 0.2–0.8 in 2xYT medium (per liter: 16 g tryptone, 10 g yeast extract, 5 g NaCl, and 100 mg ampicillin) with shaking (220 rpm). The medium was cooled to room temperature (21°C) prior to addition of 0.1 mM isopropyl-β-D-galactopyranoside to induce protein expression. After 5 h of moderate shaking (100–130 rpm), the cells were harvested by centrifugation (13,000 rpm, 4°C; 25 min), suspended in 50 mM Tris-HCl (pH 7.6)/5 mM EDTA/10% glycerol or 0.05 M $KHPO_4$ (pH 7.5)/0.3 M NaCl/0.1 M KCl/1 mM GSH/0.1% (v/v) Tween-20 with lysozyme (about 0.5 mg/ml) and, in some experiments, DNase I (about 0.1 mg/ml). The suspension was frozen and thawed twice and then sonicated (Bioruptor Next Gen; 10 times (30 s sonication, 30 s pause), 4°C). Cell debris was removed by centrifugation and the supernatants were used immediately or stored at −80°C until needed. EAS28473, EGP83657, and EGP87976 were expressed in more than three independent experiments.

We confirmed that cell lysate of untransformed *E. coli* BL21 Star cells does not oxidize 18:2*n*-6 to any of the products discussed below. Analysis of cell lysates of transformed *E. coli* without added 18:2*n*-6 did not form any metabolites of this acid.

Enzyme assays

Recombinant proteins of the crude cell lysate [in 0.05 M Tris-HCl (pH 7.6)/5 mM EDTA/10% glycerol or 0.05 M $KHPO_4$ (pH 7.5)/0.3 M NaCl/0.1 M KCl/1 mM GSH/0.1% (v/v) Tween-20] were incubated with 50–100 μM fatty acids or 30–100 μM hydroperoxides for 40 min on ice; in trapping experiments the hydroperoxides were only incubated for 1 min. The reactions (0.3–0.5 ml) were terminated with 10 ml water and the metabolites were immediately extracted on octadecyl silica (SepPak/C_{18}). The latter was washed with water and retained metabolites were eluted with ethyl acetate (4 ml). After being evaporated to dryness under N_2, the residue was dissolved in ethanol (50–100 μl), and 10 μl were subjected to LC-MS/MS analysis.

Nitrogen powder of mycelia of *Z. tritici* was homogenized in 0.1 M $KHPO_4$ buffer (pH 7.3)/2 mM EDTA/0.04% (v/v) Tween-20. The supernatant, after centrifugation at 16,200 *g* (10 min, 4°C) was incubated with 100 μM fatty acids for 30 min on ice. The products were extracted as above.

LC-MS analysis

RP-HPLC with MS/MS analysis was performed with a Surveyor MS pump (ThermoFisher) and an octadecyl silica column (5 μm; 2 × 150 mm; Phenomenex), which was eluted at 0.3–0.4 ml/min with methanol/water/acetic acid, 750/250/0.05. The effluent was subject to electrospray ionization in a linear ion trap mass spectrometer (LTQ, ThermoFisher). The heated transfer capillary was set at 315°C, the ion isolation width at 1.5 amu (5 amu for analysis of ^{2}H-labeled metabolites and hydroperoxides), the collision energy at 35 (arbitrary scale), and the tube lens at about −110 V. $PGF_{1\alpha}$ was infused for tuning. Samples were injected manually (Rheodyne 7510) or by an autosampler (Surveyor Autosampler Plus; ThermoFisher).

Normal-phase (NP)-HPLC with MS/MS analysis was performed with a silicic acid column (5 μm Reprosil; 2 × 250 mm; Dr. Maisch) using hexane/isopropyl alcohol/acetic acid, 98/2/0.01 for separation of oxidized fatty acids (0.5 ml/min; Constametric 3200 pump, LDC/MiltonRoy). The effluent was combined with isopropyl alcohol/water (3/2; 0.25 ml/min) from a second pump (Surveyor MS pump). The combined effluents were introduced by electrospray ionization into the ion trap mass spectrometer above.

Chiral-phase (CP)-HPLC analysis of 8- and 9-HPODE was performed by chromatography on Reprosil Chiral-NR (8 μm; 2 × 250 mm; Dr. Maisch), which was eluted at 0.5 ml/min with hexane/isopropyl alcohol/acetic acid, 98.8/1.2/0.01 (25), and isomers of 8-HODE were resolved on Chiralcel OBH (26). Isomers of HETE and 9- and 13-HODE were resolved on Reprosil Chiral-AM (5 μm; 2 × 250 mm; Dr. Maisch), eluted (0.2 ml/min) with hexane/methanol/acetic acid, 96/4/0.02 or 95/5/0.02. The effluents of the CP-HPLC columns were mixed with isopropyl alcohol/water in a ratio of 2:1 and electro sprayed into the mass spectrometer.

Triphenylphosphine (TPP) in hexane was used to reduce hydroperoxy fatty acids to hydroxy fatty acids. $NaBH_4$ or $NaB^{2}H_4$ in

methanol (1 mg/ml on ice; 1 h) were routinely used to reduce ketones to alcohols (27). For rapid reduction of the ^{18}O-labeled α-ketol, we added the 1 min incubation to distilled water (4°C; 1 h) with $NaBH_4$ (1 M final concentration; 1 h) and reduced foaming by low speed centrifugations. Hydrogenation was performed in ethanol with Pd/C and a gentle stream of H_2 for 2 min and the catalyst was then removed by filtration.

Bioinformatics

The ClustalW algorithm was used for sequence alignments (Lasergene, DNASTAR, Inc.). The MEGA6 software was used for construction of phylogenetic trees with 200 bootstrap tests of the resulting nodes (28).

RESULTS

Catalytic properties of EAS28473 (8*R*-DOX-AOS) of *C. immitis*

Recombinant EAS28473 oxidized 18:1*n*-9, 18:2*n*-6, and 18:3*n*-3 to 8-hydroperoxy metabolites with MS^3 spectra as reported (29, 30). The MS^2 spectra of the corresponding alcohols showed the strong and characteristic signal at *m/z* 157 [$^-$OOC-$(CH_2)_6$-CHO]. The RP-HPLC-MS/MS analysis of the oxidation of 18:2*n*-6 is shown in **Fig. 2A**. Steric analysis by CP-HPLC-MS/MS analysis (Reprosil Chiral-NR) showed that 8-HPODE had the same retention time as authentic [$^{13}C_{18}$]8*R*-HPODE (inset in Fig. 2A).

The 8*R*-hydroperoxides of 18:1*n*-9, 18:2*n*-6 and 18:3*n*-3 were further transformed to α-ketols. The 18:2*n*-6 was oxidized to 8*R*-HPODE and an α-ketol, which was identified below as 8-hydroxy-9-oxo-12*Z*-octadecenoic acid (Fig. 2A). NP-HPLC-MS/MS analysis showed that small amounts of *erythro* and *threo* 8(9)-epoxy-10-hydroxy-12*Z*-octadecenoic acids could also be detected (Fig. 2B). The MS^2 spectra (*m/z* 311→full scan) of these epoxy alcohols showed intense signals at *m/z* 157 [$^-$OOC-$(CH_2)_6$-CHO] and *m/z* 187 [$^-$OOC-$(CH_2)_6$-CHOH-CHO] as described (31).

The structure of the α-ketols formed from 18:2*n*-6 were confirmed by reduction of the ketone to a hydroxyl group, hydrogenation of the 12*Z* double bond, comparison with the mass spectra of the [$^{13}C_{18}$]-labeled α-ketol (27), and with the mass spectra of the α-ketol formed from 18:1*n*-9.

Treatment of 8-hydroxy-9-oxo-12*Z*-octadecenoic acid with NaB^2H_4 yielded *threo* and *erythro* [9-^{2}H]8,9-dihydroxy-12*Z*-octadecenoic acid (8,9-DiHODE). Their MS^2 spectra (*m/z* 314→full scan) were identical with strong signals at *m/z* 157 [$^-$OOC-$(CH_2)_6$-CHO] and *m/z* 188 [$^-$OOC-$(CH_2)_6$-CHOH-C^{2}HO] (Fig. 2C).

The 8-hydroxy-9-oxo-octadecanoic acid, which was formed by hydrogenation of 8-hydroxy-9-oxo-12*Z*-octadecenoic acid, and the α-ketol formed by oxidation of 18:1*n*-9 by recombinant EAS28473 yielded identical mass spectra (Fig. 2D). The MS^2 spectrum (*m/z* 313→full scan) of 8-hydroxy-9-oxo-octadecanoic acid showed mid-range signals, among other things, at *m/z* 183 [possibly HC(O)-C(O^-)=CH-C_8H_{17}], *m/z* 157 [$^-$OOC-$(CH_2)_6$-CHO], and *m/z* 155 (183-28; loss of CO), which supports the proposed fragmentation between C-7 and C-8, and in the upper range at *m/z* 295 (313-18),

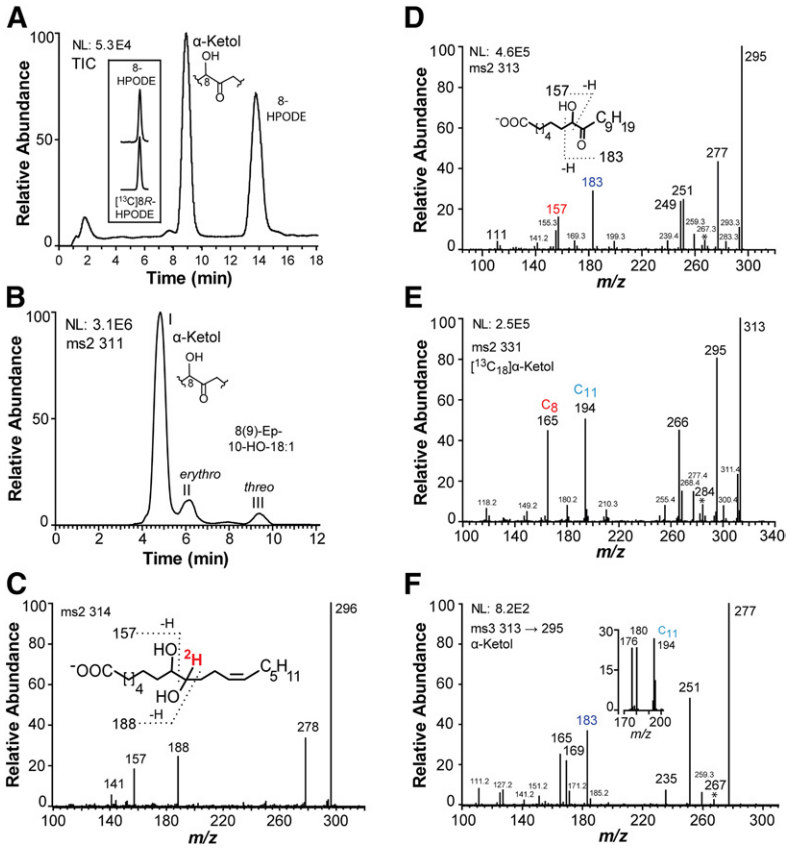

Fig. 2. RP- and NP-HPLC-MS/MS analysis of oxylipins formed from 18:2*n*-6 and 18:1*n*-9 by recombinant EAS28473 (8*R*-DOX-EAS). A: RP-HPLC-MS/MS analysis of products formed from 18:2*n*-6 by EAS28473 with major metabolites as indicated. The inset shows that 8-HPODE has the same retention time as [$^{13}C_{18}$]8*R*-HPODE on CP-HPLC (Reprosil Chiral-NR). B: NP-HPLC-MS/MS analysis of products with a molecular mass of 311 (after reduction of hydroperoxides to alcohols with TPP). The products in peaks II and III yielded the same MS^2 spectra as reported for 8(9)-epoxy-10-hydroxy-12*Z*-octadecenoic acid (labeled 8(9)-ep-10-HO-18:1) (31). C: MS/MS spectrum of the 8,9-diol formed from the α-ketol (8-hydroxy-9-oxo-12*Z*-octadecenoic acid) after reduction with $NaBH_4$. This yielded two isomers (*erythro* and *threo*) of [9-^{2}H]8,9-DiHODE with identical mass spectra. D: MS/MS spectrum of the α-ketol (8-hydroxy-9-oxo-octadecanoic acid) formed by oxidation of 18:1*n*-9 by EAS28473. E: MS/MS spectrum of [$^{13}C_{18}$]8-hydroxy-9-oxo-octadecanoic acid (obtained by hydrogenation of [$^{13}C_{18}$]8-hydroxy-9-oxo-12*Z*-octadecenoic acid). F: MS^3 spectrum of 8-hydroxy-9-oxo-octadecanoic acid (obtained by hydrogenation of 8-hydroxy-9-oxo-12*Z*-octadecenoic acid). The inset shows ions in the MS^3 spectrum of [$^{13}C_{18}$]8-hydroxy-9-oxo-octadecanoic acid between *m/z* 170 and 200. The number of carbon atoms of some fragment ions is marked $C_{subscript}$. The ions at *m/z* 267, 284 (267+17), and 267, which are formed by loss of 46 (CO+water), 29 (^{13}CO), and 28 (CO) from the carboxylate anions in (D), (E), and (F), respectively, are marked *.

JOURNAL OF LIPID RESEARCH

m/z 277 (313-2 × 18), *m/z* 267 (313-18-28; loss of water and CO), *m/z* 251 (313-44-18), and *m/z* 249, 239, and 199. Reduction of 8-hydroxy-9-oxo-octadecanoic acid with NaB^2H_4 yielded the expected signals at *m/z* 157 [$^-$OOC-$(CH_2)_6$-CHO] and *m/z* 188 [$^-$OOC-$(CH_2)_6$-CHOH-C^{2}HO]. The MS^2 spectrum (*m/z* 331→full scan) of [$^{13}C_{18}$]8-hydroxy-9-oxo-octadecanoic acid is shown in Fig. 2E. This compound was obtained by hydrogenation of the α-ketol formed from [$^{13}C_{18}$]18:2*n*-6. The fragmentation was consistent with the deduced structure, with signals at *m/z* 165 (157+9) and *m/z* 194 (183+11) as indicated in the figure.

The MS^3 spectrum (*m/z* 313→295→full scan) of 8-hydroxy-9-oxo-octadecanoic acid (Fig. 2F) showed signals at *m/z* 277 (295-18), *m/z* 267 (295-28; loss of CO), *m/z* 251 (295-44), and in the lower range *m/z* 183, 169, and 165. The MS^3 spectrum of the [$^{13}C_{18}$]8-hydroxy-9-oxo-octadecanoic acid showed that the corresponding ions in the lower mass range at *m/z* 194, 180, and 176 (inset in Fig. 2F). We conclude that 18:1*n*-9 and 18:2*n*-6 are sequentially oxidized at C-8 to hydroperoxides and dehydrated to unstable allene oxides, which are hydrolyzed to α-ketols with 8-hydroxy-9-oxo configurations.

MS/MS and MS^3 analysis of unsaturated α-ketols formed by 8*R*-DOX-AOS

The MS/MS spectra of unsaturated α-ketols, which are formed from 9-hydroperoxy fatty acids, show only weak informative signals, whereas their MS^3 spectra are more characteristic (27). We therefore investigated the MS/MS and MS^3 spectra of α-ketols derived from 8-hydroperoxy fatty acids.

The MS analyses of 8-hydroxy-9-oxo-12*Z*-octadecenoic and [$^{13}C_{18}$]8-hydroxy-9-oxo-12*Z*-octadecenoic acids are summarized in **Fig. 3**. The MS^2 spectrum of 8-hydroxy-9-oxo-12*Z*-octadecenoic acid (*m/z* 311→full scan) showed important signals at *m/z* 157 [$^-$OOC-$(CH_2)_6$-CHO], *m/z* 181 [possibly HC(O)-C(O^-)=CH-C_8H_{15}], and *m/z* 187 [$^-$OOC-$(CH_2)_6$-CHOH-CHO] as indicated by the inset in Fig. 3A. A characteristic signal of α-ketols was also noted at *m/z* 265 (A^--46; likely loss of CO and water) and *m/z* 181. The MS^2 spectrum (*m/z* 312→full scan) of [11*S*-^{2}H]8-hydroxy-9-oxo-12*Z*-octadecenoic acid showed that a strong signal at *m/z* 182 (181+1) (Fig. 3B), which supported the fragmentation. In addition, we used MS^3 and MS^4 spectra to confirm the origin of the signal at *m/z* 181. The MS^3 (*m/z* 311→181→full scan) and MS^4 spectra (*m/z* 311→293→181→full scan) of 8-hydroxy-9-oxo-12*Z*-octadecenoic acid yielded strong signals at *m/z* 163 (35%; 181-18) and *m/z* 153 (base peak, 100%; 181-28; loss of CO). These results were consistent with cleavage between C-7 and C-8 with formation of *m/z* 181 [possibly HC(O)-C(O^-)=CH-C_8H_{15}] (inset in Fig. 3A).

Some signals were likely formed by rearrangement mechanisms, e.g., *m/z* 199 (Fig. 3A). The MS^3 spectrum (*m/z* 311→199→full scan) yielded *m/z* 181 (35%; 199-18), *m/z* 155 (100%; 199-44), and *m/z* 137 (40%; 155-18) as the major fragment ions.

MS^3 spectra of α-ketols often contain strong and characteristic signals and can be useful complements to the MS/MS spectra, although the complex MS^3 fragmentation is difficult to interpret. The MS^3 spectrum of 8-hydroxy-9-oxo-12*Z*-octadecenoic acid (*m/z* 311→293→full scan) showed prominent signals at *m/z* 265 (293-28), *m/z* 181,

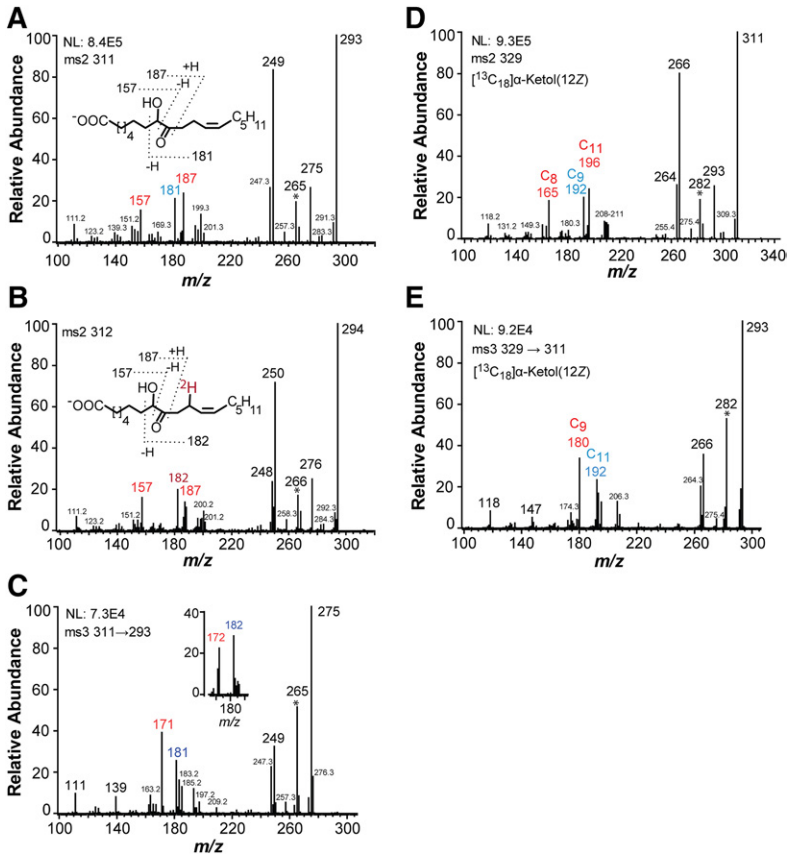

Fig. 3. MS/MS and MS^3 spectra of the α-ketol (8-hydroxy-9-oxo-12*Z*-octadecenoic acid) formed from 18:2*n*-6 and [$^{13}C_{18}$]18:2*n*-6 by recombinant EAS28473 (8*R*-DOX-AOS). A: MS/MS spectrum of 8-hydroxy-9-oxo-12*Z*-octadecenoic acid. B: MS/MS spectrum of the monodeuterated α-ketol, [11*S*-^{2}H]8-hydroxy-9-oxo-12*Z*-octadecenoic acid. C: MS^3 spectrum of 8-hydroxy-9-oxo-12*Z*-octadecenoic acid. D: MS^3 spectrum of [$^{13}C_{18}$]8-hydroxy-9-oxo-12*Z*-octadecenoic acid. E: MS^3 spectrum of [$^{13}C_{18}$]8-hydroxy-9-oxo-12*Z*-octadecenoic acid. The number of carbon atoms of some fragment ions is marked $C_{subscript}$ in (E). Important fragments are labeled in a larger font and colored. NL, intensity normalized to 100%. The ions at *m/z* 282 in (D) and (E), which are likely formed by loss of 47 (^{13}CO+water) and 29 (^{13}CO), respectively, are marked *.

and *m/z* 171 (Fig. 3C), whereas the corresponding spectrum (*m/z* 311→293→full scan) of [11*S*-^{2}H]8-hydroxy-9-oxo-12*Z*-octadecenoic acid yielded many signals increased by one mass unit, notably in the lower mass range at *m/z* 182 (181+1) and *m/z* 172 (171+1) (inset in Fig. 3C).

We finally recorded the MS/MS and MS^3 spectra of the [$^{13}C_{18}$]8-hydroxy-9-oxo-12*Z*-octadecenoic acid for comparison with these spectra of the unlabeled compound. The MS^2 spectrum (*m/z* 329→full scan) of [$^{13}C_{18}$]8-hydroxy-9-oxo-12*Z*-octadecenoic acid showed signals, among other things, at *m/z* 165 (see 157+8), *m/z* 196 (see 187+9), *m/z* 192 (see 181+11), and weak signals at *m/z* 208–211 of equal intensities (Fig. 3D). The MS^3 spectrum (*m/z* 329→311→full scan) of the [$^{13}C_{18}$]8-hydroxy-9-oxo-12*Z*-octadecenoic acid showed strong signals, among other things, at *m/z* 282 (311-29; loss of ^{13}CO), *m/z* 192, and *m/z* 180, which likely contained 17, 11, and 9 carbon atoms (Fig. 3E). This confirmed the proposed fragmentation.

The 8*R*-DOX-AOS differs from 9*R*-DOX-AOS of Aspergilli by transforming 18:3*n*-3 via 8*R*-HPOTrE to an allene oxide/α-ketol (**Fig. 4A**). The structure of the α-ketol was confirmed by LC-MS analysis before and after hydrogenation.

The MS^2 spectrum (*m/z* 309→full scan) of the α-ketol with two double bonds, 8-hydroxy-9-oxo-12*Z*,15*Z*-octadecadienoic acid, showed signals, among other things, at *m/z* 157, 179, and 197 (see inset in Fig. 4B). The fragmentation ion at *m/z* 179 was supported by the MS^3 spectrum (*m/z* 309→291→179→full scan; data not shown), which yielded *m/z* 161 (179-18) and *m/z* 151 (179-28; loss of CO) in analogy with the corresponding ion at *m/z* 181 in the MS/MS spectrum of 8-hydroxy-9-oxo-12*Z*-octadecenoic acid discussed above (see Fig. 3A). The signal at *m/z* 197 might be due to rearrangement. The MS^4 spectrum (*m/z* 309→291→197→full scan) yielded *m/z* 179 (197-18) and *m/z* 153 (197-44) as the main ions.

The MS^3 spectrum (*m/z* 309→291→full scan) of the α-ketol showed signals, which were not present in the MS/MS spectrum, e.g., at *m/z* 193, 171, and 165. The MS^4 spectrum (*m/z* 309→291→193→full scan; data not shown) yielded signals at *m/z* 175 (193-18) and *m/z* 165 (193-28; loss of CO) (Fig. 4B), suggesting that *m/z* 193 and 165 could be related.

Finally, the structure of the α-ketol formed from 18:3*n*-3 was confirmed by LC-MS analysis after hydrogenation to 8-hydroxy-9-oxo-octadecanoic acid (see Fig. 2D).

The 18:3*n*-6 appeared to be a poor substrate in analogy with 8*R*-DOX-LDS. The 20:2*n*-6 was oxidized at C-11, but transformation to α-ketols could not be detected. The product specificity suggested that recombinant EAS28473 could be named 8*R*-DOX-AOS with 18:1*n*-9, 18:2*n*-6, and 18:3*n*-3 as likely natural substrates.

Oxidation of arachidonic acid by 8*R*-DOX-AOS of *C. immitis*

C. immitis is a human pathogen and we therefore also assessed the oxidation of 20:4*n*-6 by 8*R*-DOX-AOS. The metabolites were reduced with TPP and analyzed by NP- and CP-HPLC-MS/MS (supplemental Fig. S1A, B). The three main products were identified as 8-, 10-, and 12-HETE

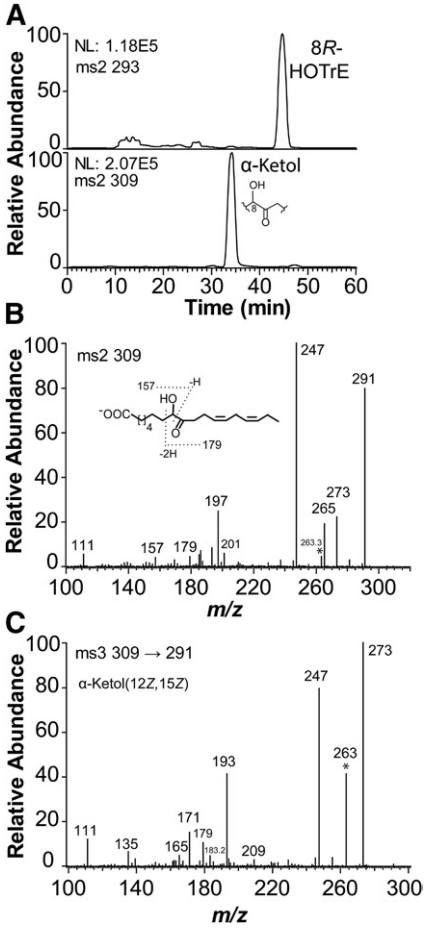

Fig. 4. NP-HPLC-MS/MS analysis of oxylipins formed from 18:3*n*-3 by EAS28473 (8*R*-DOX-AOS). A: NP-HPLC-MS/MS analysis. The top chromatogram shows elution of 8-HPOTrE and the bottom chromatogram shows elution of the α-ketol, 8-hydroxy-9-oxo-12*Z*,15*Z*-octadecadienoic acid. B: MS/MS spectrum of 8-hydroxy-9-oxo-12*Z*,15*Z*-octadecadienoic acid. C: MS^3 spectrum of 8-hydroxy-9-oxo-12*Z*,15*Z*-octadecadienoic acid. The ions at *m/z* 263, which are formed by loss of 46 (CO+water) and 28 (CO) in (B) and (C), respectively, are marked *. NL, intensity normalized to 100%.

from their MS^2 spectra (*m/z* 419→full scan), which were as reported previously (32). Steric analysis showed that both 12-HETE and 8-HETE mainly consisted of the *S* stereoisomers, as judged from reanalysis with added authentic 12*S*-HETE and 8*R*-HETE. The minor product, 10-HETE, eluted on CP-HPLC mainly as a single isomer (95%), but the stereo configuration was not further investigated.

Catalytic properties of recombinant EGP83657 (8*S*-DOX-AOS) of *Z. tritici*

EGP83657 oxidized 18:1*n*-9, 18:2*n*-6, and 18:3*n*-3 to 8-hydroperoxy metabolites and to α-ketols in analogy with 8*R*-DOX-AOS, but with an important difference. Steric analysis of 8-HPODE showed that it mainly consisted of the *S* stereoisomer (**Fig. 5A**), which apparently was sequentially converted to 8*S*(9)-epoxy-9,12*Z*-octadecadienoic acid [8*S*(9)-EODE] and then hydrolyzed to an α-ketol.

The 8*S*-HPODE was formed from [8*R*-^{2}H]18:2*n*-6 with retention of the deuterium label (Fig. 5B). These observations

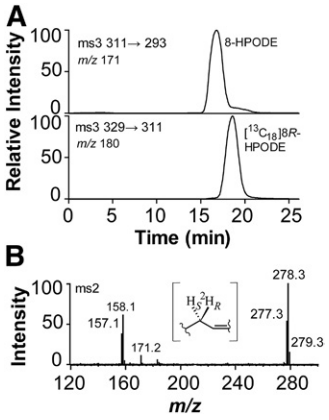

Fig. 5. Steric analysis of 8-HPODE formed by EGP83657 (8*S*-DOX-AOS) and the retention of deuterium during oxidation of [8*R*-^{2}H]18:2*n*-6 to 8*S*-HPODE. A: The 8-HPODE formed by EGP83657 eluted before [$^{13}C_{18}$]8*R*-HPODE on the CP-HPLC column and it was thus identified as the 8*S* stereoisomer. B: MS/MS spectrum (*m/z* 293–297→full scan) of 8-HODE formed from [8*R*-^{2}H]18:2*n*-6 (65% ^{2}H) (33). The even numbered fragments contain the ^{2}H label, and the signal at *m/z* 158 is likely due to the fragment ion $^-$OOC-$(CH_2)_6$-C^{2}HO. The inset shows the labeling of hydrogens at C-8 of 18:2*n*-6.

are consistent with suprafacial hydrogen abstraction and oxygen insertion, whereas 8*R*-DOX catalyzes antarafacial hydrogen abstraction and oxygenation as discussed above (33).

The 20:2*n*-6 was oxidized at C-11, but an α-ketol could not be detected. The 18:3*n*-6 was a poor substrate. We conclude that EGP83657 can be described as 8*S*-DOX-AOS with 18:1*n*-9, 18:2*n*-6, and 18:3*n*-3 as likely natural substrates.

Catalytic properties of recombinant EGP87976 (9*R*-DOX-AOS) of *Z. tritici*

Recombinant EGP87976 oxidized 18:2*n*-6 and transformed 9*R*-HPODE to two polar products, as judged by RP-HPLC-MS analysis (peaks I and II in supplemental Fig. S2A). The MS/MS and MS^3 spectra were as reported for the γ- and α-ketols, respectively, of 9-HPODE-derived allene oxides (27). The 18:2*n*-6 was also oxidized to 9-HPODE, and steric analysis by CP-HPLC (Reprosil Chiral-AM) and MS^2 analysis showed that 9-HPODE consisted of the 9*S* and 9*R* stereoisomers in a ratio of ~1:3 (supplemental Fig. S2B). This underestimates the relative formation of the 9*R* stereoisomer as 9*R*-HPODE was further transformed to α- and γ-ketols as major products.

The 18:3*n*-3 was a poor substrate, and 9*S*-HPODE was transformed mainly to epoxy alcohols, but a 9-HPODE-derived α-ketol was also detected by its characteristic MS^3 spectrum (27). Recombinant EGP87976 thus belongs to the group of 9*R*-DOX-AOS, which is found in Aspergilli (Fig. 1B).

Oxidation of fatty acids by mycelia of *Z. tritici*

Nitrogen powder of mycelia of *Z. tritici* oxidized 18:1*n*-9, 18:2*n*-6, and 18:3*n*-3 to hydroperoxides at C-8 and to variable amounts of 5,8-diols. Steric analysis (Chiralcel OBH) showed that 8*R*-HPODE stereoisomer was formed (>95%), and the 5,8-diols were identified by two characteristic fragments formed by MS/MS analysis, *m/z* 115 [$^-$OOC-(CH_2)-CHO] and *m/z* 173 [$^-$OOC-$(CH_2)_3$-CHOH-$(CH_2)_2$-CHO]. The oxidation of 18:2*n*-6 to hydroperoxides by nitrogen powder of *Z. tritici* is shown in **Fig. 6A**. In addition to 8-HPODE, large amounts of 13-HPODE were also detected. Steric analysis with aid of [$^{13}C_{18}$]13-HODE showed that 13*S*-HPODE was the main stereoisomer (>98%; inset in supplemental Fig. S2A). The 18:3*n*-3 was also oxidized at C-13, but 18:1*n*-6 was not. The oxidation at C-13 of 18:2*n*-6 and 18:3*n*-3 was therefore likely catalyzed by 13*S*-LOX. We could not detect formation of α-ketols.

EGP91582 aligns with 8*R*-DOX-LDS, and this protein is a strong candidate for the observed 5,8-LDS activities. The oxidation at C-13 of 18:2*n*-6 and 18:3*n*-3 was likely due to the only LOX of *Z. tritici* (GenBank identification number: EGP90986), which belongs to the family of fungal iron LOX (Fig. 6B). The 13*S*-LOX of *Z. tritici* thus has the same

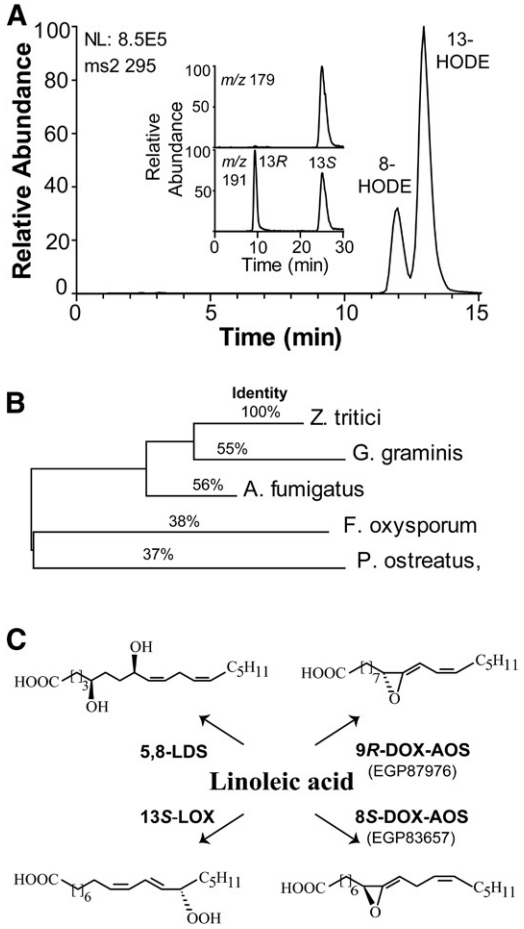

Fig. 6. The 13*S*-LOX and 5,8-LDS activities of mycelia and an overview of fatty acid DOXs of *Z. tritici*. A: RP-HPLC-MS/MS analysis of hydroperoxides after reduction to alcohols. The inset shows that 13S-HODE was the main product (top) as judged from the separation of ^{13}C-labeled 13*R*- and 13*S*-HODE (bottom). B: Phylogenetic tree of five iron LOXs. The GenBank identification numbers are (from top to bottom): EGP90986, EJT77580, EAL84806, EKX38530, and BAI99788. The phylogenetic tree was constructed with MEGA6. The percent sequence identity with EGP90986 is indicated. C: Overview of the oxidation of 18:2*n*-6 by mycelia (left) and by two recombinant DOX-AOSs (right) of *Z. tritici*.

catalytic activity as reported for the LOX of *Fusarium oxysporum* and *Pleurotus ostreatus* (8, 34).

A summary of the oxidation of 18:2*n*-6 by mycelia and by 8*S*- and 9*R*-DOX-AOS is shown in Fig. 6C. The DOX-AOS activities could not be detected in mycelia and may only be expressed in response to environmental stimuli in analogy with other secondary metabolites.

Non-enzymatic hydrolysis of allene oxides

It seems likely that the α-ketols, which are derived from oxidation of 18:2*n*-6, are formed from nonenzymatic hydrolysis of allene oxides, 8*R*(9)- and 8*S*(9)-epoxy-10,12*Z*-octadecadienoic acids [8*R*(9)- and 8*S*(9)-EODE] (18). Hydrolysis of allene oxides to α-ketols occurs mainly with inversion of configuration of the hydroxyl group compared with the configuration of the precursor hydroperoxide (17, 35, 36). The two α-ketols, which are formed by hydrolysis of 8*R*(9)- and 8*S*(9)-EODE, are therefore expected to consist mainly of the 8*S*- and 8*R*-hydroxy-9-oxo-12*Z*-octadecenoic acids, respectively.

CP-HPLC-MS/MS analysis showed that 8*R*(9)-EODE and [$^{13}C_{18}$]8*S*(9)-EODE were hydrolyzed to α-ketols with different retention times (**Fig. 7A**). The stereoisomer with the shortest retention time was formed by hydrolysis of 8*R*(9)-EODE and thus tentatively identified as the α-ketol with 8*S* configuration. "*S* before *R*" is also the elution order of the major α-ketols formed by hydrolysis of 9*R*(10)- and 9*S*(10)-EODE, respectively (17).

Hydrolysis of allene oxides in an excess of methanol will form methoxy derivatives. We incubated 8*R*-DOX-AOS for 1 min with excess 8*R*-HPODE, added 30 vol of methanol and let the hydrolysis proceed for 1 h. To facilitate the analysis, we reduced the α-ketols with $NaBH_4$. Analysis showed the presence of the expected products, 8,9-DiHOME and 8-methoxy-9-hydroxy-12*Z*-octadecenoic acid, in a ratio of ~9:1 (Fig. 7B). The MS/MS spectrum (*m/z* 327→full scan) of the latter is shown in Fig. 7C. Signals were noted at *m/z* 309 (327-18), *m/z* 295 (327-32; loss of methanol), *m/z* 277 (295-18), and *m/z* 201 [$^{-}$OOC-$(CH_2)_6$-CHOCH$_3$-CHO], and in the lower mass range at *m/z* 186, 171, and 141. The MS^3 spectrum (*m/z* 327→201→full scan) showed signals at *m/z* 186 (100%; 201-15, loss of ·CH_3) and *m/z* 169 (10%; 201-32, loss of methanol), whereas MS^3 spectrum (*m/z* 327→295→full scan) yielded intense signals at *m/z* 277 (100%; 295-18), *m/z* 171 (35%), and *m/z* 141 (20%). These spectra were consistent with the proposed structure. The trapping experiment indicates a short half time of the unconjugated allene oxide, 9*R*(10)-EODE, as about 90% was hydrolyzed by water after 1 min of incubation (Fig. 7B).

We next analyzed the transformation of [$^{18}O_2$]8*R*-HPODE by 8*R*-DOX-AOS to determine the incorporation of ^{18}O into the α-ketol (8-hydroxy-9-oxo-12*Z*-octadecenoic acid). The ketone at C-9 of the α-ketol can be exchanged with water and we therefore reduced the products formed after 1 min with $NaBH_4$. LC-MS analysis of *erythro* and *threo* 8,9-DiHODE in the full scan mode showed incorporation of one molecule of ^{18}O (Fig. 7D) and the MS^2 spectrum (*m/z* 315→full scan) showed a signal at *m/z* 189, which demonstrated the ^{18}O-label at C-9 (Fig. 7E).

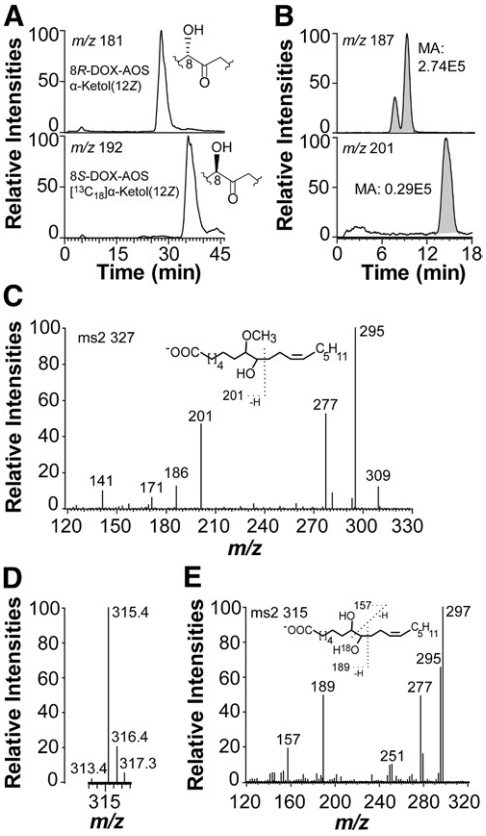

Fig. 7. Analysis of hydrolysis products of allene oxides. A: CP-HPLC-MS/MS analysis of stereoisomers of α-ketols. The α-ketols were formed from 18:2*n*-6 and [$^{13}C_{18}$]18:2*n*-6 by 8*R*- and 8*S*-DOX-AOS, respectively. Hydrolysis of 9-HPODE-derived allene oxides is known to result in inversion of configuration at C-9 (35). The 9*S*-α-ketol elutes before the 9*R*-α-ketol on CP-HPLC (Reprosil Chiral-AM) (17). The α-ketols formed from 8*R*- and 8*S*-DOX-AOS eluted in the same order, 8*S*-hydroxy-9-oxo-octadecenoic before [$^{13}C_{18}$]8*R*-hydroxy-9-oxo-octadecenoic acid, as illustrated by the insets in the two chromatograms. B: RP-HPLC analysis of products formed by 8*R*-DOX-AOS after incubation for 1 min with 8*R*-HPODE and then terminated with methanol (30 vol; 60 min at 21°C.). The α-ketols were reduced to alcohols ($NaBH_4$) before analysis. The top chromatogram shows separation of *erythro* and *threo* isomers of 8,9-DiHOME [monitoring of *m/z* 187; $^{-}$OOC-$(CH_2)_6$-CHOH-CHO] and the bottom chromatogram shows elution of 8-methoxy-9-hydroxy-12*Z*-octadecenoic acids (monitoring of *m/z* 201 [187+14; $^{-}$OOC-$(CH_2)_6$-CHOCH$_3$-CHO] in a broad peak. MA, measured area as indicated in gray. C: MS/MS spectrum of 8-methoxy-9-hydroxy-12*Z*-octadecenoic acid. The inset demonstrates the ion at *m/z* 201. D: Hydrolysis of allene oxides formed from [$^{18}O_2$]8*R*-HPODE by 8*R*-DOX-AOS. The partial mass spectrum after reduction with $NaBH_4$ to 8,9-DiHODE shows the intensities of the carboxylate anions with (*m/z* 315) and without (*m/z* 313) the ^{18}O-label. E: MS/MS analysis of [^{18}O]8,9-DiHODE. The inset shows the fragmentation.

Transformation of hydroperoxides by 8*R*- and 8*S*-DOX-AOS

The transformation of other hydroperoxides by 8*R*- and 8*S*-DOX-AOS may indicate their relation to other AOS of fungi. We therefore assessed whether the 8*R*-AOS of 8*R*-DOX-AOS (EAS28473) and 8*S*-AOS of 8*S*-DOX-AOS (EGP83657) could transform 9- and 13-HPODE.

The 8*R*-DOX-AOS efficiently transformed 9*R*-HPODE to an epoxy alcohol as a major product, but an α-ketol

could not be detected. The epoxy alcohol was tentatively identified as *threo* 9*R*(10*R*)-epoxy-11-hydroxy-12*Z*-octadecenoic acid, as judged from NP- and RP-HPLC-MS/MS analysis (*m/z* 311→full scan) (31) along with small amounts of the *erythro* isomer (supplemental Fig. S3A). The 9*S*-, 13*S*-, and 13*R*-HPODE were only converted to small fractions (5–10%) of epoxy alcohols, as judged by RP-HPLC-MS/MS analysis.

The 8*S*-DOX-AOS (EGP83657) converted only a fraction of 8*R*-HPODE to 8-hydroxy-9-oxo-12*Z*-octadecenoic acid (5–10%). In contrast, about 50% of 9*S*-HPODE was transformed to an α-ketol, 9-hydroxy-10-oxo-12*Z*-octadecenoic acid, and to *erythro* and *threo* 9*S*(10*S*)-epoxy-11-hydroxy-12Z-octadecenoic acids (supplemental Fig. S3B) [see (31)]. The relative amounts of the α-ketol and the epoxy alcohols were ∼1:2. The 9*S*-HPOTrE was transformed in the same way. The α-ketols were identified by their characteristic MS^2 and MS^3 spectra (16, 27). The 9*R*-HPODE and 13*S*- and 13*R*-HPODE were not transformed by 8*S*-DOX-AOS, as only small amounts of epoxy alcohols were detected (<10%).

The transformation of 9*S*-HPODE by the 8*S*-AOS activities to an α-ketol, which originates from 9*S*(10)-EODE, suggests that the 8*S*-AOS may have evolved from 9*S*-AOS of 9*S*-DOX-AOS.

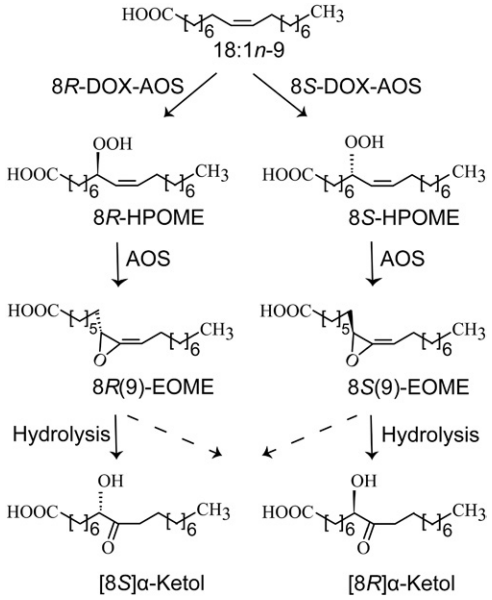

Fig. 8. Overview of the sequential oxidation of oleic acid to 8-hydroperoxyoctadecenoic acid (HPOME) and to allene oxides by 8*R*- and 8*S*-DOX-AOS. The two allene oxides, 8*R*(9)- and 8*S*(9)-epoxy-9-octadecamonoenoic acids (EOMEs), are mainly hydrolyzed to α-ketols by inversion of configuration at C-8 (solid arrows).

DISCUSSION

Our main goal was to investigate the catalytic properties of three putative DOX-CYP fusion enzymes of *C. immitis* (EAS28473) and *Z. tritici* (EGP83657 and EGP87976). We report that two of the recombinant enzymes form novel allene oxides and they are named 8*R*- and 8*S*-DOX-AOS, respectively, whereas the third enzyme belongs to the 9*R*-DOX-AOS subfamily. The sequential oxidation of 18:1*n*-9 by 8*R*- and 8*S*-DOX-AOS to allene oxides and hydrolysis to α-ketols are outlined in **Fig. 8**. We detected 5,8-LDS and 13*S*-LOX activities of mycelia of *Z. tritici* (Fig. 6C), which could be attributed to expression of EGP91582 and EGP90986, respectively.

Previously described allene oxides are formed from *cis-trans* conjugated hydroperoxy fatty acids, e.g., from 9*S*- and 13*S*-HPOTrE by plant CYP74, 8*R*-hydroperoxyeicosatetraenoic acid by the AOS-LOX of the coral, *Plexaura homomalla*, and from 9*R*- and 9*S*-HPODE by fungal 9-DOX-AOS (37–39). The allene oxides can be transformed enzymatically or nonenzymatically to cyclopentenone fatty acids, e.g., analogs of jasmonic acid and prostaglandin A_2, respectively (37–39). The process leading to a cyclopentenone from the 10*Z*-isomer of the 9*S*-HPODE-derived allene oxide was recently studied in detail (40, 41). This allene oxide undergoes homolytic cleavage with formation of a ketone at C-10, a radical at C-9, and an allyl-like radical at C-11 to C-13. This oxyallyl diradical may then form a cyclopentenone. In contrast, 8-HPODE-derived allene oxides lack conjugated double bonds, but they are nevertheless rapidly hydrolyzed by methanol or water (Fig. 7). The oxidation of 18:1*n*-9 to allene oxides by 8-DOX-AOS is unprecedented as this fatty acid is a poor substrate of LOXs and fungal 9*R*- and 9*S*-DOX-AOSs (17, 42).

The 8*R*- and 8*S*-DOX-AOS can be aligned with 51% amino acid identity, but the four amino acids in the 8-DOX domains from the catalytic Tyr to the proximal His heme ligand are not identical. The consensus sequence TyrArg-**Phe**His of all 9*S*- and 9*R*-DOX domains is conserved in 8*R*-DOX-AOS, but it is replaced in 8*S*-DOX-AOS with the consensus sequence TyrArg**Trp**His of 8*R*-DOX-LDS, 10*R*-DOX-(CYP), and 10*R*-DOX-EAS. 8*S*-DOX-AOS is, nevertheless, the first described enzyme with a catalytic 8*S*-DOX domain.

The substrate recognition sites (SRSs) 4 (or I-helices) of the 8*R*- and 8*S*-AOS domains differ. The hexamer SRS 4 sequence ValAlaThrGlnAlaGln of 8*R*-AOS aligns except for one or two positions (in bold type) with the SRS 4 sequence ValAla**Asn**Gln(**Ala**/**Gly**)Gln of 5,8-LDS [see (18, 43)]. The CYP domain of 8*S*-DOX-AOS is catalytically related to 9*S*-DOX-AOS, as it transformed 9*S*-HPODE to an α-ketol, but this relation is not evident from SRS 4 or other sequence alignments of 8*S*- and 9*S*-AOS domains.

The general rule for oxygenation of unsaturated fatty acids by COXs, LOXs, and DOX-CYP fusion enzymes is antarafacial hydrogen abstraction and oxygen insertion. Exceptions to this rule are, for example, fungal LOXs with catalytic manganese, 9*R*-DOX, and 9*R*-DOX-AOS (6, 17, 20). The 9*R*- and 9*S*-DOX-AOSs both abstract the *proR* hydrogen at C-11 of 18:2*n*-6, but oxygen is inserted from opposite directions. An outline of the sequential biosynthesis of 8*S*-HPODE and 8*S*(9)-EODE from 18:2*n*-6 by 8*S*-DOX-AOS and the nonenzymatic hydrolysis of 8*S*(9)-EODE to an α-ketol is shown in **Fig. 9A**. Due to the Cahn-Ingold-Prelog rule, the *proR* hydrogen at C-11 points in the same direction as the *proS* hydrogen at C-8 of 18:2*n*-6, which is abstracted

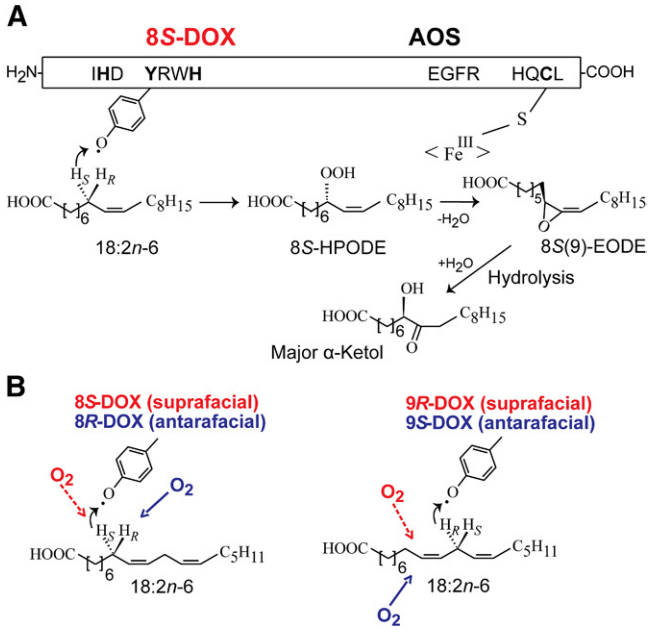

Fig. 9. Illustration of the sequential biosynthesis of allene oxides from 18:2*n*-6 by 8*S*-DOX-EAS (EGP83657) and the suprafacial and antarafacial oxidation mechanisms of 8- and 9-DOX-AOS. A: Overview of the sequential biosynthesis of allene oxides by 8*S*-DOX-AOS and important amino acid residues for catalysis. B: The 8*S*- and 8*R*-DOX-AOSs abstract the *proS* hydrogen at C-8, whereas 9*S*- and 9*R*-DOX-AOSs abstract the *proR* hydrogen at C-11. The figure illustrates that these *proS* and *proR* hydrogens have the same absolute configuration relative to the 9*Z*,12*Z*-pentadiene structure. The red and blue arrows indicate the direction of oxygen insertion at C-8 and C-9, respectively, in relation to the pentadiene structure. The *S* and *R* assignments are due to the Cahn-Ingold-Prelog nomenclature rule.

by both 8*R*- and 8*S*-DOX-AOS (Fig. 9B). The 8*S*-DOX-AOS thus catalyzes suprafacial hydrogen abstraction and oxygenation in analogy with 9*R*-DOX-AOS.

Interestingly, 9*R*-DOX-AOS of *Aspergillus niger* can be transformed to 9*S*-DOX-AOS by replacement of two amino acids with those conserved in these two positions of 9*S*-DOX-AOS, Gly616Ile and Phe626Leu (17). This shifts the direction of oxygenation, but it does not change the hydrogen abstraction (see Fig. 9B). Gly616 and Phe627 were not conserved in the corresponding positions of either 8*S*-DOX-AOS or 8*R*-DOX-AOS, which both contain Leu residues in these positions.

What is the biological function of 8-DOX-AOS? *C. immitis* and its closely related species, *Coccidioides posadasii*, cause common and potentially serious human infections, which are endemic in California and Arizona (21). It was therefore of interest to determine whether 8*R*-DOX-AOS could metabolize arachidonic acid, as eicosanoids have potent actions in inflammation and its resolution (44). Arachidonic acid was transformed to 8*S*-, 10-, and 12*S*-hydroperoxyeicosatetraenoic acid. None of these metabolites are known to have specific biological effects (44), but it would be of interest to determine whether 8*R*-DOX-AOS is expressed during infection of human cells and metabolizes arachidonic acid of the host.

Z. tritici is spread worldwide, and septoria tritici blotch is often considered to be the most devastating disease of wheat (22, 23). Plants transform 13*S*-HPOTrE sequentially to allene oxides and to jasmonates, which act as growth and defense hormones (37, 38). The fungal AOS domains can only be aligned with plant AOSs (CYP74) and related P450 with a low degree of amino acid identity (18). Fungal AOSs and CYP74 have likely evolved independently. The parallel evolution of 8*R*-, 8*S*-, 9*R*-, and 9*S*-DOX-AOSs in fungi and CYP74 linked to LOX in plants suggest that the allene oxides may be of biological importance. This is well-established in the pathway to jasmonic acid with potent actions in plants (37, 38). *Lasiodiplodia theobromae* and a few other fungal pathogens overproduce jasmonic acid to induce pathological plant growth (45). Fungal jasmonates may be formed by the biochemical pathway in plants, but details are lacking (8, 46). The fungal repertoire of oxylipins likely participates in the struggle between the pathogen and its host, as well as in reproduction and development (1).

In summary, we have characterized fatty acid oxygenases of *Z. tritici* and report biosynthesis of two novel allene oxides formed by 8*R*- and 8*S*-DOX-AOS of *C. immitis* and *Z. tritici*. Their natural substrates are likely unsaturated C_{18} fatty acids, and the biological function of these secondary metabolites should be evaluated in the context of related allene oxides formed by plants.

The authors are grateful for the generous help, advice, and the deuterated fatty acids provided by Dr. Hamberg, the Karolinska Institute, Stockholm, Sweden.

REFERENCES

1. Tsitsigiannis, D. I., and N. P. Keller. 2007. Oxylipins as developmental and host-fungal communication signals. *Trends Microbiol.* **15:** 109–118.
2. Brodhun, F., and I. Feussner. 2011. Oxylipins in fungi. *FEBS J.* **278:** 1047–1063.
3. Funk, C. D. 2001. Prostaglandins and leukotrienes: advances in eicosanoid biology. *Science.* **294:** 1871–1875.
4. Newcomer, M. E., and A. R. Brash. 2015. The structural basis for specificity in lipoxygenase catalysis. *Protein Sci.* **24:** 298–309.
5. Su, C., and E. H. Oliw. 1998. Manganese lipoxygenase. Purification and characterization. *J. Biol. Chem.* **273:** 13072–13079.
6. Hamberg, M., C. Su, and E. Oliw. 1998. Manganese lipoxygenase. Discovery of a bis-allylic hydroperoxide as product and intermediate in a lipoxygenase reaction. *J. Biol. Chem.* **273:** 13080–13088.
7. Wennman, A., A. Magnuson, M. Hamberg, and E. H. Oliw. 2015. Manganese lipoxygenase of Fusarium oxysporum and the structural basis for biosynthesis of distinct 11-hydroperoxy stereoisomers. *J. Lipid Res.* **56:** 1606–1615.
8. Brodhun, F., A. Cristobal-Sarramian, S. Zabel, J. Newie, M. Hamberg, and I. Feussner. 2013. An iron 13S-lipoxygenase with an alpha-linolenic acid specific hydroperoxidase activity from Fusarium oxysporum. *PLoS One.* **8:** e64919.
9. Hörnsten, L., C. Su, A. E. Osbourn, P. Garosi, U. Hellman, C. Wernstedt, and E. H. Oliw. 1999. Cloning of linoleate diol synthase reveals homology with prostaglandin H synthases. *J. Biol. Chem.* **274:** 28219–28224.
10. Xiao, G., A. L. Tsai, G. Palmer, W. C. Boyar, P. J. Marshall, and R. J. Kulmacz. 1997. Analysis of hydroperoxide-induced tyrosyl radicals and lipoxygenase activity in aspirin-treated human prostaglandin H synthase-2. *Biochemistry.* **36:** 1836–1845.
11. Su, C., M. Sahlin, and E. H. Oliw. 1998. A protein radical and ferryl intermediates are generated by linoleate diol synthase, a ferric hemeprotein with dioxygenase and hydroperoxide isomerase activities. *J. Biol. Chem.* **273:** 20744–20751.

12. Brodowsky, I. D., M. Hamberg, and E. H. Oliw. 1992. A linoleic acid (8R)-dioxygenase and hydroperoxide isomerase of the fungus Gaeumannomyces graminis. Biosynthesis of (8R)-hydroxylinoleic acid and (7S,8S)-dihydroxylinoleic acid from (8R)-hydroperoxylinoleic acid. *J. Biol. Chem.* **267:** 14738–14745.
13. Su, C., and E. H. Oliw. 1996. Purification and characterization of linoleate 8-dioxygenase from the fungus Gaeumannomyces graminis as a novel hemoprotein. *J. Biol. Chem.* **271:** 14112–14118.
14. Hoffmann, I., F. Jernerén, U. Garscha, and E. H. Oliw. 2011. Expression of 5,8-LDS of Aspergillus fumigatus and its dioxygenase domain. A comparison with 7,8-LDS, 10-dioxygenase, and cyclooxygenase. *Arch. Biochem. Biophys.* **506:** 216–222.
15. Hoffmann, I., F. Jernerén, and E. H. Oliw. 2014. Epoxy alcohol synthase of the rice blast fungus represents a novel subfamily of dioxygenase-cytochrome P450 fusion enzymes. *J. Lipid Res.* **55:** 2113–2123.
16. Hoffmann, I., and E. H. Oliw. 2013. Discovery of a linoleate 9S-dioxygenase and an allene oxide synthase in a fusion protein of Fusarium oxysporum. *J. Lipid Res.* **54:** 3471–3480.
17. Sooman, L., A. Wennman, M. Hamberg, I. Hoffmann, and E. H. Oliw. 2016. Replacement of two amino acids of 9R-dioxygenase-allene oxide synthase of Aspergillus niger inverts the chirality of the hydroperoxide and the allene oxide. *Biochim. Biophys. Acta.* **1861:** 108–118.
18. Hoffmann, I., F. Jernerén, and E. H. Oliw. 2013. Expression of fusion proteins of Aspergillus terreus reveals a novel allene oxide synthase. *J. Biol. Chem.* **288:** 11459–11469.
19. Jernerén, F., A. Sesma, M. Franceschetti, M. Hamberg, and E. H. Oliw. 2010. Gene deletion of 7,8-linoleate diol synthase of the rice blast fungus: studies on pathogenicity, stereochemistry, and oxygenation mechanisms. *J. Biol. Chem.* **285:** 5308–5316. [Erratum. 2010. *J. Biol. Chem.* **285:** 20422.]
20. Sooman, L., and E. H. Oliw. 2015. Discovery of a novel linoleate dioxygenase of Fusarium oxysporum and linoleate diol dynthase of Colletotrichum graminicola. *Lipids.* **50:** 1243–1252.
21. Nguyen, C., B. M. Barker, S. Hoover, D. E. Nix, N. M. Ampel, J. A. Frelinger, M. J. Orbach, and J. N. Galgiani. 2013. Recent advances in our understanding of the environmental, epidemiological, immunological, and clinical dimensions of coccidioidomycosis. *Clin. Microbiol. Rev.* **26:** 505–525.
22. O'Driscoll, A., S. Kildea, F. Doohan, J. Spink, and E. Mullins. 2014. The wheat-Septoria conflict: a new front opening up? *Trends Plant Sci.* **19:** 602–610.
23. Goodwin, S. B., S. B. M'Barek, B. Dhillon, A. H. Wittenberg, C. F. Crane, J. K. Hane, A. J. Foster, T. A. Van der Lee, J. Grimwood, A. Aerts, et al. 2011. Finished genome of the fungal wheat pathogen Mycosphaerella graminicola reveals dispensome structure, chromosome plasticity, and stealth pathogenesis. *PLoS Genet.* **7:** e1002070.
24. Hamberg, M. 2011. Stereochemistry of hydrogen removal during oxygenation of linoleic acid by singlet oxygen and synthesis of 11(S)-deuterium-labeled linoleic acid. *Lipids.* **46:** 201–206.
25. Garscha, U., T. Nilsson, and E. H. Oliw. 2008. Enantiomeric separation and analysis of unsaturated hydroperoxy fatty acids by chiral column chromatography-mass spectrometry. *J. Chromatogr. B Analyt. Technol. Biomed. Life Sci.* **872:** 90–98.
26. Garscha, U., and E. H. Oliw. 2007. Steric analysis of 8-hydroxy- and 10-hydroxyoctadecadienoic acids and dihydroxyoctadecadienoic acids formed from 8R-hydroperoxylinoleic acid by hydroperoxide isomerases. *Anal. Biochem.* **367:** 238–246.
27. Jernerén, F., Hoffmann, I., and Oliw, E. H. (2010) Linoleate 9R-dioxygenase and allene oxide synthase activities of Aspergillus terreus. *Arch. Biochem. Biophys.* **495:** 67–73. [Erratum. 2010. *Arch. Biochem. Biophys.* **500:** 210.]
28. Tamura, K., G. Stecher, D. Peterson, A. Filipski, and S. Kumar. 2013. MEGA6: molecular evolutionary genetics analysis version 6.0. *Mol. Biol. Evol.* **30:** 2725–2729.
29. Oliw, E. H., A. Wennman, I. Hoffmann, U. Garscha, M. Hamberg, and F. Jernerén. 2011. Stereoselective oxidation of regioisomeric octadecenoic acids by fatty acid dioxygenases. *J. Lipid Res.* **52:** 1995–2004.
30. Oliw, E. H., C. Su, T. Skogström, and G. Benthin. 1998. Analysis of novel hydroperoxides and other metabolites of oleic, linoleic, and linolenic acids by liquid chromatography-mass spectrometry with ion trap MSn. *Lipids.* **33:** 843–852.
31. Oliw, E. H., U. Garscha, T. Nilsson, and M. Cristea. 2006. Payne rearrangement during analysis of epoxyalcohols of linoleic and alpha-linolenic acids by normal phase liquid chromatography with tandem mass spectrometry. *Anal. Biochem.* **354:** 111–126.
32. Bylund, J., J. Ericsson, and E. H. Oliw. 1998. Analysis of cytochrome P450 metabolites of arachidonic and linoleic acids by liquid chromatography-mass spectrometry with ion trap MS. *Anal. Biochem.* **265:** 55–68.
33. Hamberg, M., L. Y. Zhang, I. D. Brodowsky, and E. H. Oliw. 1994. Sequential oxygenation of linoleic acid in the fungus Gaeumannomyces graminis: stereochemistry of dioxygenase and hydroperoxide isomerase reactions. *Arch. Biochem. Biophys.* **309:** 77–80.
34. Tasaki, Y., S. Toyama, T. Kuribayashi, and T. Joh. 2013. Molecular characterization of a lipoxygenase from the basidiomycete mushroom Pleurotus ostreatus. *Biosci. Biotechnol. Biochem.* **77:** 38–45.
35. Hamberg, M. 2000. New cyclopentenone fatty acids formed from linoleic and linolenic acids in potato. *Lipids.* **35:** 353–363.
36. Brash, A. R. 2009. Mechanistic aspects of CYP74 allene oxide synthases and related cytochrome P450 enzymes. *Phytochemistry.* **70:** 1522–1531.
37. Gfeller, A., L. Dubugnon, R. Liechti, and E. E. Farmer. 2010. Jasmonate biochemical pathway. *Sci. Signal.* **3:** cm3.
38. Wasternack, C., and E. Kombrink. 2010. Jasmonates: structural requirements for lipid-derived signals active in plant stress responses and development. *ACS Chem. Biol.* **5:** 63–77.
39. Song, W. C., and A. R. Brash. 1991. Investigation of the allene oxide pathway in the coral Plexaura homomalla: formation of novel ketols and isomers of prostaglandin A2 from 15-hydroxyeicosatetraenoic acid. *Arch. Biochem. Biophys.* **290:** 427–435.
40. Hebert, S. P., J. K. Cha, A. R. Brash, and H. B. Schlegel. 2016. Investigation into 9(S)-HPODE-derived allene oxide to cyclopentenone cyclization mechanism via diradical oxyallyl intermediates. *Org. Biomol. Chem.* **14:** 3544–3557.
41. Brash, A. R., W. E. Boeglin, D. F. Stec, M. Voehler, C. Schneider, and J. K. Cha. 2013. Isolation and characterization of two geometric allene oxide isomers synthesized from 9S-hydroperoxy-linoleic acid by P450 CYP74C3: Stereochemical assignment of natural fatty acid allene oxides. *J. Biol. Chem.* **288:** 20797–20806.
42. Clapp, C. H., M. Strulson, P. C. Rodriguez, R. Lo, and M. J. Novak. 2006. Oxygenation of monounsaturated fatty acids by soybean lipoxygenase-1: Evidence for transient hydroperoxide formation. *Biochemistry.* **45:** 15884–15892.
43. Hoffmann, I., and E. H. Oliw. 2013. 7,8- and 5,8-linoleate diol synthases support the heterolytic scission of oxygen-oxygen bonds by different amide residues. *Arch. Biochem. Biophys.* **539:** 87–91.
44. Haeggström, J. Z., and C. D. Funk. 2011. Lipoxygenase and leukotriene pathways: biochemistry, biology, and roles in disease. *Chem. Rev.* **111:** 5866–5898.
45. Jernerén, F., F. Eng, M. Hamberg, and E. H. Oliw. 2012. Linolenate 9R-dioxygenase and allene oxide synthase activities of Lasiodiplodia theobromae. *Lipids.* **47:** 65–73.
46. Tsukada, K., K. Takahashi, and K. Nabeta. 2010. Biosynthesis of jasmonic acid in a plant pathogenic fungus, Lasiodiplodia theobromae. *Phytochemistry.* **71:** 2019–2023.